Journal of Applied Mechanics and Technical Physics, Vol. 46, No. 6, pp. 901–910, 2005

NEW X-RAY TECHNIQUES FOR FLOW VISUALIZATION AND MEASUREMENT OF HYDRODYNAMIC FLOW PARAMETERS IN OPAQUE HETEROGENEOUS MEDIA

E. I. Bichenkov,* E. I. Palchikov, S. V. Sukhinin, A. N. Cheremisin, A. I. Romanov, M. A. Romanyuta, and K. S. Seleznev

UDC 01-203, 01-327, 02-211

This paper proposes and validates a method for the quantitative analysis of multiphase flows and objects of complex composition with image registration on a charge-coupled-device array taking into account the X-ray spectral characteristics. The method was tested on objects of known composition and shape. New approaches are formulated to solve a number of research problems related to the use of modern registration techniques and computer-based tools for X-ray image processing.

Key words: *X-rays, spectral distribution, absorption, photodetector, CCD array, digital image processing, tomography, filtration, multicomponent fluid.*

INTRODUCTION

The X-ray technique ranks high among the various methods for studying material motion and its spatial distribution. In many cases, it seems to be a single method that provides reliable information on research objects. This is true for studies of the processes involved in explosion, high-velocity impact, material behavior under conditions of sever radiation interferences, in the case of shielding of the examined samples by opaque walls or material flows, etc.

X-ray tomographic techniques have been developed and tested long enough ago [1, 2]. They turned out to be complicated and expensive. Therefore, simple X-ray techniques still dominate both research studies and production plants [3]. The most extensively used techniques are one-dimensional X-ray densitometry [4, 5] or shadow photography, which allows one to obtain not too accurate information on the dimensions and shape of the photographed object and material distribution from the photographic density of a photograph or the dynamics of the process from several photographs taken at different times. The devices of [4] use the simple linear model of radiation absorption developed in [6] assuming that the radiation is monochromatic. Spectral characteristics are incorporated in the model but the computations are performed for a very approximate model of low accuracy which requires additional calibrations.

The modern status of the instrumentation, circuitry, and computer technology together with the level and body of accumulated knowledge of the interaction of X-rays with matter make it possible to change the emphasis in formulating problems related to the development of new methods of quantitative radiography. We see prospects

*Deceased.

Lavrent'ev Institute of Hydrodynamics, Siberian Division, Russian Academy of Sciences, Novosibirsk 630090; palchikov@hydro.nsc.ru. Translated from Prikladnaya Mekhanika i Tekhnicheskaya Fizika, Vol. 46, No. 6, pp. 159–170, November–December, 2005. Original article submitted September 16, 2004.

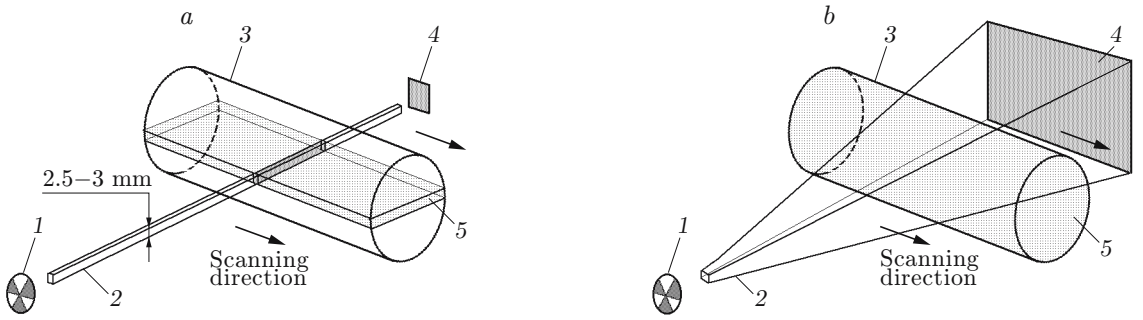

Fig. 1. Scanning diagram: (a) one-dimensional scanning; (b) two-dimensional scanning with a shift; 1) X-ray source; 2) collimated radiation beam; 3) sample; 4) radiation detector; 5) measurement region.

for the development of new methods of research radiography in performing studies in two directions: 1) the use of modern registration systems and computer-based image processing tools to increase the information content, accuracy, and reliability of measurements without complicating the experimental facility; 2) the development of measurement procedures that take into account the spectral distribution of the emission from X-ray sources, the absorption spectra of the materials constituting the object under study, and the spectral characteristics of the detector, which can also be used to increase the information content and measurement accuracy. Some results from studies in these directions are given in the present paper.

UPDATING OF THE RADIOGRAPHIC DEVICE

At present there are a number of conventional devices for studying samples under slowly (quasistatically) varying conditions. An example of such processes is the filtration of one or several fluids in a porous medium with a rigid matrix; interest in these processes is motivated by the importance of such studies for solving a number of oil production problems.

The concentrations of various fluids in porous material samples are usually measured by scanning along its diameter by a narrow X-ray beam about 3 mm wide and high. In this case, the experimental conditions allow the X-ray source and the radiation detector located at the opposite end of the sample to be moved synchronously along the sample [4, 5]. As a result, one obtains an axial concentration distribution (or a diagram of the sample saturation with the fluid). The scale length of such a diagram is determined by the width of the beam in which data accumulation occurs and by the resolution of the trolley position. Facilities developed using this design (Fig. 1a) are in essence X-ray densitometers and give one-dimensional axial distributions of materials.

The replacement of the recording detector by a detector array [usually a charge-coupled-device (CCD) array with a phosphor strip, which converts the X-rays to visible light] considerably increases the information content of the experiment. The images obtained by this device are substantially two-dimensional and cannot provide information on the three-dimensional structure of the sample and the three-dimensional flow pattern.

Twenty years ago, the creation of a photosensitive array with image decomposition into hundreds of elements was the technological peak in the development of multi-element detectors. At present, two-dimensional photosensitive CCD arrays with millions of elements on their surface have been developed and put into commercial production. The use of these arrays is the next step in research radiography. A significant advantage of CCD arrays is that in modern commercial image recording devices, the image is represented in digitized form with a large number of brightness measurement levels for each element, a high degree of repeatability, and a high linearity of the transmission characteristic, i.e., with a very high accuracy. Even more than ten years ago, CCD arrays surpassed photographic film in the dynamic range and linearity by three orders of magnitude [7].

The array eliminates the use of expensive and deficient X-ray films and provides a high-quality flash photograph of a certain phase of a pulsed process with noise limited only by the quantum nature of the signal. In the case of fairly slow processes, by shifting the object relative to the source and detector, one can obtain a series of images on one array and use them for further calculations.

A scanning device with recording a series of conical projections of a sample is shown in Fig. 1b. For each cross section of the sample, one obtains a set of oblique projections sufficient for constructing tomographic sections of the sample.

USING SPECTRAL CHARACTERISTICS TO INCREASE THE MEASUREMENT ACCURACY AND CAPABILITIES

Circuitry and Metrological Basis for New Measurement Techniques. The measuring channel of any X-ray device consists of a radiation source, an object being studied, and a radiation detector. Let us sequentially analyze the current knowledge of the spectral characteristics and accuracy of these three basic units of the measuring channel and the capabilities of modern image recording tools for the most effective use of this knowledge.

Radiation Source. The measured spectra of various X-ray apparatus and methods of their simulation are described in [8, 9]. A fairly thorough review of the results obtained, measurement techniques, and methods for computing the spectra of such devices is given in [10].

Great advances have been made in the development of methods for calculating bremsstrahlung spectra. An important recent finding should be noted at this point. It turns out that the interaction mechanism between an electron of given energy and an atom is now so well known that a Monte Carlo simulation for only 1000 histories yields a bremsstrahlung spectrum with a relative standard deviation of not more than 5%, i.e., within the standard experimental accuracy. This technique was tested at the Budker Institute of Nuclear Physics, Siberian Division, Russian Academy of Sciences.

The emission spectra of stationary X-ray apparatus stabilized for the operating voltage and current have been studied most thoroughly.

The situation with pulsed devices is much worse. The spectral distribution of the emission from such devices have not been measured, the stability of their pulses is insignificant, and reliable computational models are not available. The emission from such devices is usually judged by the accumulated dose measured by a dosimeter and by the thickness of the scanned layer of a widely used metals, such as iron, aluminum, etc. Such measurements are of a qualitative nature. An important advance was measurements of the flash period and the dose rate of some X-ray flash devices [11]. The foregoing is sufficient to understand that the development of well tested techniques for measuring the emission spectra of flash devices is an independent research challenge.

Interaction of Radiation with a Sample and Radiation Absorption. The radiation absorption by all elements of the Periodic Table and many compounds have been well studied, classified, and published. Today, in addition to the traditional sources of information there are ample opportunities for information communication through network communication channels. Several web sites provide a large body of data on the interaction of X-rays with matter. The mass absorption coefficients used in the present study were obtained from the Internet database server at the National Institute of Standards and Technology (NIST), Gaithersburg, MD, USA [12].

X-Ray Image Recording System. To convert X-ray images to optical one, we used a rare earth phosphor screen based on gadolinium oxysulfide Gd_2O_2S (Renex Company, Novosibirsk, Russia). The absorption and attenuation spectra of the phosphor were taken from the NIST database [12].

A Baumer Arc4000 digital CCD camera with progressive scanning was used for optical image input and digitization. The camera has a 2/3-inch optical sensor, the cell (pixel) size is 6.7×6.7 μm, and the image size is 1300×1030 pixels. The camera exposure is in the range of 200 μsec to 10 sec, and the signal-to-noise ratio without cooling is better than 60 dB. The camera provides a single-shot digitization accuracy of 12 bits — 4096 gray gradations.

The foregoing leads to the conclusion that there is a reliable circuitry and metrological basis for the development of measurement procedures that take into account the spectrum of the radiation source, the absorption spectra of the materials constituting the examined objects, and the spectral characteristics of the detector.

BASIC PROPOSITIONS FOR NUMERICAL CALCULATIONS

Absorption Model. The calculations were based on the conventional model of exponential attenuation of monochromatic X-rays in a homogeneous medium with the attenuation coefficient dependent on the wavelength and

properties of the material, i.e., the intensity of the monochromatic radiation transmitted through a homogeneous object was described by the expression

$$J = J_0 \exp\Big(- \int\limits_L \frac{\mu}{\rho}(p)\, \rho\, dp\Big).$$

Here $(\mu/\rho)(p)$ is the X-ray mass attenuation coefficient at the point p, J_0 is the initial radiation intensity, and ρ is the material density.

For nonmonochromatic sources, it is necessary to take into account the dependence of the mass attenuation coefficient on energy. In the case of a finite number of the homogenous materials constituting the scanned object, in the conventional linear model, we have

$$J(E) = I_0(E) \exp\Big(- \sum_i \frac{\mu_i}{\rho_i}(E)\, \rho_i x_i\Big), \tag{1}$$

where $(\mu_i/\rho_i)(E)$ is the mass attenuation coefficient of radiation of energy E for the ith material, x_i is the thickness of the material with number i along the beam, ρ_i is the density of the ith material, and $I_0(E)$ is the initial intensity of radiation of energy E (emission spectrum of the X-ray apparatus).

Expression (1) is approximate. It does not incorporate the spatial distribution of the material along the X-ray propagation direction. Because soft X-rays are absorbed more strongly than hard X-rays, the spectral distribution of the radiation changes in passing a material layer and the intensity of the X-rays transmitted through a compound sample should depend on the relative position of the different materials. Accounting for this factor significantly complicates the problem. In the present study, the use of this model for the radiation interaction with the examined object is justified by the fact that we used an X-ray source with an operating voltage of 70–160 kV and the energy of the generated X-rays was concentrated mainly in the range of 40–140 keV. In this range there is no sharp increase in the attenuation coefficients, as is the case in the range of energies of <10–15 keV, and the attenuation coefficients vary insignificantly.

The CCD camera registers the light intensity of the phosphor, which is proportional to the X-ray energy absorbed by the phosphor. With allowance for the absorption in the examined sample, the intensity of the radiation transmitted through the phosphor is given by

$$J(E) = I_0(E) \exp\Big(- \sum_i \frac{\mu_i}{\rho_i}(E)\, \rho_i x_i\Big) \exp\Big(- \frac{\mu_l}{\rho_l}(E)\, \rho_l d_l\Big), \tag{2}$$

and the radiation absorbed by the phosphor is defined by the difference of (1) and (2):

$$\Delta J(E) = I_0(E) \exp\Big(- \sum_i \frac{\mu_i}{\rho_i}(E)\, \rho_i x_i\Big)\Big[1 - \exp\Big(- \frac{\mu_l}{\rho_l}(E)\, \rho_l d_l\Big)\Big]. \tag{3}$$

Here $(\mu_l/\rho_l)(E)$ is the mass absorption coefficient and ρ_l and d_l are the density and thickness of the phosphor material, respectively.

The CCD camera measures the pixel brightness. It can be obtained by integrating (3) over the source spectrum:

$$A = K \int\limits_{E_{\min}}^{E_{\max}} I_0(E) \exp\Big(- \sum_i \frac{\mu_i}{\rho_i}(E)\, \rho_i x_i\Big)\Big[1 - \exp\Big(- \frac{\mu_l}{\rho_l}(E)\, \rho_l d_l\Big)\Big]\, dE. \tag{4}$$

In expression (4), K is an integral coefficient that characterizes the conversion of X-rays to light and the camera sensitivity. It needs to be determined by calibration of the measuring channel.

For several X-ray tube voltage (and, hence, different emission spectra of the X-ray apparatus), we can write the following system of equations:

$$A_n = K_n \int\limits_{E\,\min}^{E\,\max} I_n(E) \exp\Big(- \sum_i \frac{\mu_i}{\rho_i}(E)\, \rho_i, x_i\Big)\Big[1 - \exp\Big(- \frac{\mu_l}{\rho_l}(E)\, \rho_l d_l\Big)\Big]\, dE, \tag{5}$$

where n is the ordinal number of the experiment; $I_n(E)$ is the emission spectrum of the X-ray apparatus with a tube voltage E_n; and K_n is a coefficient determined by a calibration photograph.

Calculation of the Sample Density Distribution. As a result of the experiment, the CCD camera produces an output digital image of the light-intensity distribution on the phosphor screen, i.e., in (5) A_n is determined as a function of the propagation direction of the radiation registered by a given pixel. Solving (5), one can calculate the unknown spatial distribution of the material density x_i.

To improve this technique, test its accuracy and reliability, and determine additional correction coefficients due to the use of approximations in the mathematical model of the experiment, we performed test experiments in which the object thickness was determined in the case where a homogeneous material was on the path of the X-ray beam. The problem thus reduces to solving one integral equation, which contains one varied parameter x_1. The solution of this problem does not involve any difficulties and was sought by conventional methods. For this, we determined the functional $F(x_1)$

$$F(x_1) = \Big[A_1 - K \int\limits_{E\,\min}^{E\,\max} I_1(E) \exp\Big(-\frac{\mu_1}{\rho_1}(E)\,\rho_1 x_1\Big)\Big[1 - \exp\Big(-\frac{\mu_l}{\rho_l}(E)\,\rho_l d_l\Big)\Big]\,dE\Big]^2$$

and, using variations, found the distribution of x_1 that provides a minimum of $F(x_1)$. As usual, it was assumed that exactly this distribution x_1 gives a solution of the problem.

In the case of several homogenous materials, the problem reduces to solving a system of integral equations. The solution was sought in the same manner as in the previous case: introducing the functional

$$F(x_1, x_2, \ldots, x_n) = \sum_{i=1}^{n} F_i(x_i), \tag{6}$$

where

$$F_i(x_i) = \Big[A_i - K \int\limits_{E\,\min}^{E\,\max} I_i(E) \exp\Big(-\sum \frac{\mu_i}{\rho_i}(E)\,\rho_i\,x_i\Big)\Big[1 - \exp\Big(-\frac{\mu_l}{\rho_l}(E)\,\rho_l d_l\Big)\Big]\,dE\Big]^2,$$

we sought for the vector $x = \{x_1, x_2, \ldots, x_n\}$ on which $F(x_1, x_2, \ldots, x_n)$ has a minimum. This vector was taken to be a solution of the problem.

Processing of Experimental Data. The experimental-data processing and the search for a solution were divided into the following steps.

Interpolation of Supplementary Data. Cubic interpolation splines were constructed from table data (the spectrum of the X-ray apparatus, X-ray attenuation coefficients), and the spline coefficients were entered into a computer and used in calculations.

Extension of the Range of Brightness Measurements. Image averaging over pixels and CCD array binning were applied. Because of the formation mechanism of the electronic relief of CCD images, an increase in the spatial resolution leads to a decrease in the number of electrons accumulated in one photosensitive element of the CCD structure. As a result, the relative role of fluctuations in the number of electrons in the element increases and the dynamic range of the image brightness reduces. Since the total number of the array elements is very large, it is possible in some cases to sacrifice spatial resolution by performing image averaging over several cells or by combining cells on the array (binning). This reduces the noise due to fluctuations in the number of electrons in array cell and increases the range of brightness measurement. This correction of digitized images on photosensitive arrays needs to be done taking into account the spectral distribution of the recorded radiation.

In the case of heterogeneous materials, binning was implemented over areas of 2×2 or 4×4 pixels, which does not contribute additional accuracy to the spatial resolution but eliminates errors due to the discrete nature of the image and statistical fluctuations in the number of electrons during formation of the image electronic relief. The averaging was applied on large areas if this did not reduce the information content of the image, for example over all pixels on the step of the calibration wedge.

Construction of the Functional. After interpolating the supplementary data and entering the image into the computer memory, we constructed the functional $F(x_1, x_2, \ldots, x_n)$ in which the integral over the energy was replaced by a sum with the step $dE = 0.1$ keV.

Search for a Solution. The vector $x = \{x_1, x_2, \ldots, x_n\}$ that ensures a minimum of the functional $F(x_1, x_2, \ldots, x_n)$ was sought using the bisection method and the exhaustive search method for homogeneous and

heterogeneous materials, respectively. The programs were tested on virtual three-dimensional fractal-type objects. We are sincerely grateful to D. Yu. Mekhontsev, who greatly helped us in this step of the study.

Three-Phase Medium with a Known Total Thickness. For a fixed total thickness, the problem of determining the thicknesses of the components of a three-phase medium is equivalent to determining the thicknesses of a two-phase medium followed with the subsequent calculation of the third component by subtracting the two obtained functions from the known total thickness.

Tomography for a Polyenergetic Spectrum. In tomography, it is required to determine the absorption function for each point of the scanned object. To solve the problem, we partitioned the search area into cells and assumed the absorption inside each cell was constant. The problem was thus reduced to the case of a finite set of different materials along each beam L. Then for the beam L, the minimum of the functional (6) was found and $\rho_1, \rho_2, \ldots$ were determined using the methods described above. In the final step, a tomogram was constructed using algebraic methods or by projection with filtration.

TEST FACILITY AND EXPERIMENT AUTOMATION

The test facility was designed using the registration device shown in Fig. 1. The radiation source was a VIP FED160-320 system (Sintez company, St. Petersburg). This is a power supply stabilized with respect to the anode current, voltage, and radiation intensity with a built-in 0.3BPM25-150 X-ray tube (Svetlana-Rentgen company, St. Petersburg).The adjustment ranges were as follows: 70–160 kV for the tube voltage, 0.1–2.0 mA for the current, and 1–998 sec for the exposure time or it was stationary. The size of the focal spot was 0.8×0.8 mm. The instability of the current, voltage, and intensity was less than 0.5%.

We employed a Baumer Arc4000 camera, which was connected to a computer through a shielded twisted pair using a standard PCI bus interface plate. LVDS camera control was used.

The scanning–input system was driven by stepper motors with an accuracy not worse than 10 μm. The movement was controlled independently by optical gauges. The sample diameter was 30 mm, and its length was 30 to 300 mm. The sample was placed in an X-ray transparent holder made of a composite material. The anode–detector distance was 750 mm, and the sample–detector distance was 50 mm.

Since the experiment involved digitization and acquisition of thousands of images of the examined samples, it turned out to be necessary to develop a computerized experiment control system and to design the software needed for this purpose. Control of the facility and data acquisition were implemented by a P-IV computer with a 1700 MHz processor frequency, a 512 MB memory, and a 40 GB disk drive. The images are saved in the 16-bit PNG format. The facility performance, bus network and control diagrams, and the design of the X-ray image input system are described in detail in [13, 14].

TESTING OF THE TECHNIQUE

Examined Objects. The technique was tested on stepped wedges of copper, aluminum, and iron of known thickness. Photographs were taken from one or two wedges of different substances. As a model of a saturated porous medium, we used a dry sandstone sample, ahead of which water and oil wedges (Fig. 2) were placed. Such model experiments do not limit the generality of the technique but considerably simplifies the check of the results since the determination of the sample saturation is rather difficult.

One-Component Medium. The examined samples were sets of aluminum, iron, and copper plates 1, 0.35, and 1.5 mm thick. The exposure time was 3 sec, the X-ray tube voltage 120 kV, and the anode current 1.5 mA. The thicknesses for the various steps of the wedges were calculated from the results of photograph processing. Figure 3 shows curves of the thickness of the absorbing plates calculated in relative units (the y axis) versus their actual thickness (the x axis). One can see that the calculated curves are almost linear. Figure 3 also gives the linear approximation functions obtained by least-squares fitting. The correlation coefficients $R^2 = 0.9948$ for iron and $R^2 = 0.9986$ for aluminum show that the curves of the calculated thickness versus the actual thickness are linear with a probability of 99%. From Fig. 3 it is evident that for copper the curve of the calculated value versus the actual thickness deviates markedly from the liner law. An analysis of the dependence of the light intensity of the

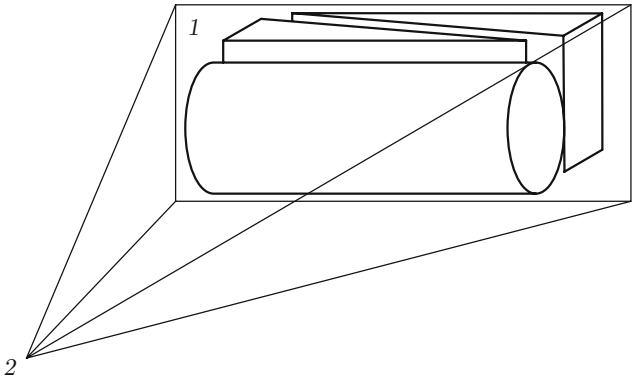

Fig. 2. Diagram of the model experiment: 1) phosphor; 2) X-ray apparatus.

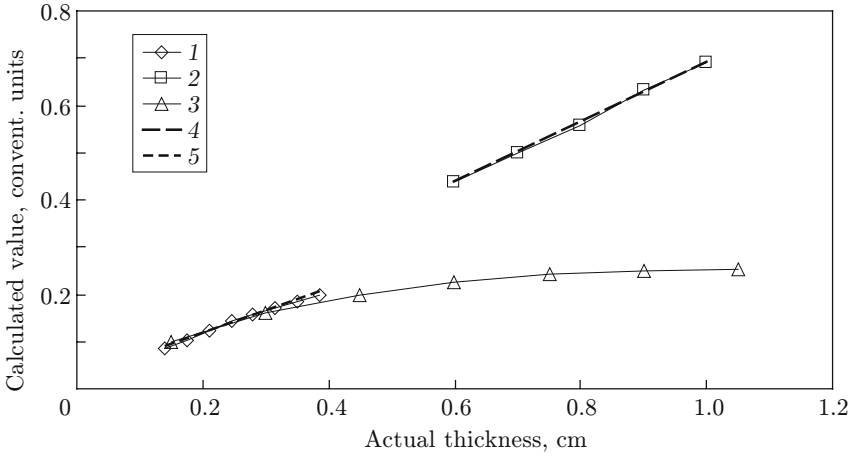

Fig. 3. Calculated thickness versus actual thickness for wedges of iron (1), aluminum (2), and copper (3); curves 4 and 5 are the linear approximations $y = 0.465x + 0.0244$ and $y = 0.64x + 0.052$, respectively.

phosphor screen on the thickness of the copper sample shows that as the thickness of the copper layer increases, the signal reaches an asymptote that corresponds to the scattered background radiation that appears. This experiment demonstrates the natural limitation of the capabilities of the developed technique.

Two-Component Medium. The quantitative multiphase X-ray technique was tested on wedges filled with two different fluids: oil and an aqueous solution of KI (a diagram of the experiment is shown in Fig. 2). The measurements were performed at X-ray tube voltages of 120 and 160 kV. The wedges were made of a Duralumin foil 50 μm thick. The radiation attenuation at this thickness was ignored.

In the case of two-component media, the solution of the problem becomes much more complicated. The standard procedures for finding the minimum of a function of two variables search only for a local minimum and require the determination of an initial approximate solution or the specification of a gradient of the function. Both of these are difficult to implement in our case. Therefore, the absolute minimum in the interval of interest to us was determined for several iterations using exhaustive search with a varied grid size.

Figure 4 gives curves of the calculated thickness versus actual thickness for wedges with KI solution and oil. They are both well fitted by straight lines.

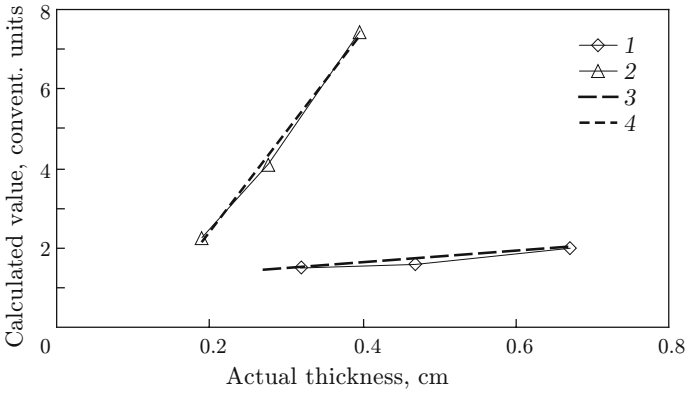

Fig. 4. Calculated thickness versus actual thickness for wedges with water and oil (between the wedges there was a porous sample): points 1 and 2 refer to KI solution and oil, respectively; curves 3 and 4 are the linear approximations $y = 25.178x - 2.6276$ and $y = 1.4687x + 0.9757$, respectively.

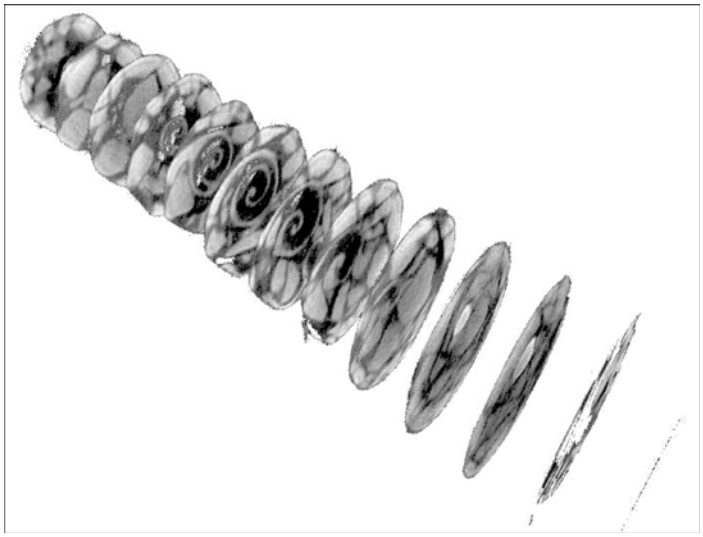

Fig. 5. Set of tomographic scans of the porous medium model.

VISUALIZATION OF FLUID-MIXTURE FLOW IN POROUS MEDIA

Test Tomographic Experiment. In our case, the state of the system is registered using a set of two-dimensional X-ray image arrays obtained by a digital CCD array. This improves the reliability of measurements of the object density and saturations in oil reservoir simulations, allows conventional and small-angle tomography to be performed, and provides information on the two and three-dimensional spatial structures of the sample and flow.

To test the tomographic method, we developed a porous medium model. The model consisted of small stones and inclusions (steel beads and seashells). The obtained scans are given in Fig. 5.

Representation of Results and Problem of Saturation Inhomogeneity. The new facilities and techniques described above give fairly accurate data on the heterogeneity structure of materials, the flow front velocity, and the fluid concentration in porous media. The detailed information on the spatial distribution of the fluid concentration obtained on real samples with their saturation and replacement of one fluid component by another has revealed a number of problems related the representation of the results [15, 16].

Three-dimensional isoconcentration surfaces calculated from a series of X-ray photographs provide a more detailed insight into the evolution of the flow front. Figure 6 show the position of the filtration front for three different times. It is evident that the front first lagged near the axis of the sample and the lag region was then

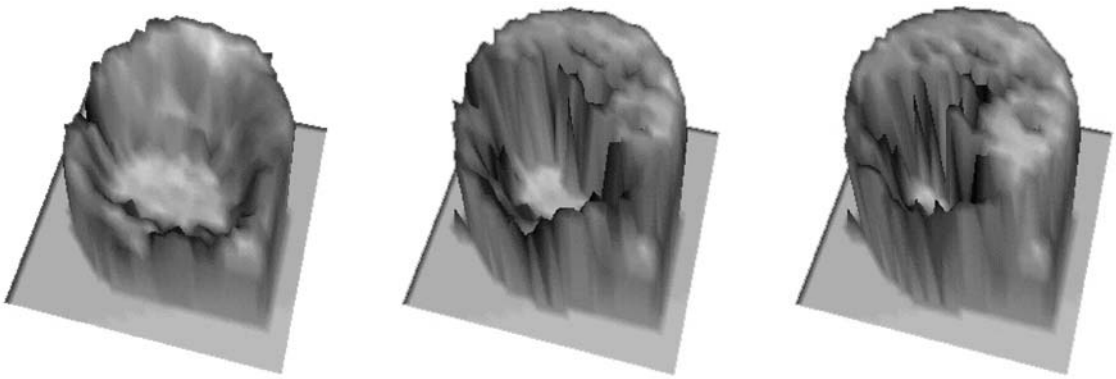

Fig. 6. Isoconcentration surfaces at various times.

shifted to one of the sides. In addition, one can see that the front has "fingers" and "curtains," which are most likely due to the presence of large capillaries in the sample.

The results presented above agree with the results of [2, 3, 14–16] obtained for problems of homogeneous saturation of porous samples with multiphase fluids. At present, because of the increasing amount of measurements of the saturation dynamics using X-ray methods, the problem has entered a new level and become more urgent, and in experiments new additional data appear that cannot be ignored. The results obtained in the present section highlight the need for a careful statistical processing of quantitative measurements of the integral saturation of samples. In such processing, it is necessary to take into account the entire sample volume, to measure the degree and characteristics of fluctuations, indicating the quantitative and qualitative degrees of data heterogeneity and their basic characteristics: the spatial spectrum of heterogeneities, the standard deviation for each component, etc.

CONCLUSIONS

A new technique of polyenergetic tomographic scanning using a series of shifted conical projections was developed and used to design a device based on an X-ray optical CCD detector for the observation of saturation of porous sample with fluids. The calculations took into account the exact spectral characteristics of the X-ray source, detector, and examined media, which reduced the number of calibrations and increased the accuracy and reliability of concentration measurements for each fluid component. All this was achieved by using modern image recording and processing tools without complicating the experimental facility. The necessary numerical calculations were performed on a conventional office computer. The large number of points in the samples in the processing of two-dimensional image arrays and the large volume of the samples for X-ray density measurements provided noise reduction and high measurement accuracy even for a one-dimensional data representation.

The designed techniques and software were tested on objects of standard shape and composition.

Experiments using the designed measurement technique showed that the filtration of fluid mixtures through porous samples is accompanied by strong fluctuations in the spatial distributions of the concentrations and filtration-front velocity, whose values increase with an increase in the dimension of the problem.

The results obtained in the present study showed the advantages and prospects for use of two-dimensional CCD arrays with an image digitization system in designing measuring complexes for studies of the multiphase fluid flow dynamics in porous media.

The study used the large conceptual and software-analytical tools created at the Lavrent'ev Institute of Hydrodynamics of the Siberian Division of the Russian Academy of Sciences and the Yukos-NOVOSIBIRSK Scientific-Educational Center at the Educational-Research Department of the Novosibirsk State University.

REFERENCES

1. H. J. Vinegar, "X-ray CT and NMR imaging of rocks," *J. Petrol. Technol.*, **38**, No. 3, 257–259 (1986).
2. E. S. Sprunt, K. P. Desal, M. E. Coles, et al., "CT-scan-monitored electrical-resistivity measurements show problems achieving homogeneous saturation," *SPE Formation Evaluation*, **6**, No. 3, 134–140 (1991).
3. V. C. Tidwell and R. J. Glass, "X-ray visible light transmission for laboratory measurement of two-dimensional saturation fields in thin-slab systems," *Water Resour. Res.*, **30**, No. 11, 2873–2882 (1994).
4. "The XRSC-198 two or three-phase X-ray core flood scanning system," Coretest Systems, Inc., 400 Woodview Av., Morgan Hill, CA 95037, USA (2005); `http://www.coretest.com/pdf/xrsc-198.pdf`.
5. "AXRP-300 automated X-ray relative permeability system," Core Laboratories. 2015 McKenzie, Suite 106, Carrollton, Texas, 75006, USA (2005); `http://www.corelab.com/coreinst/pdf/advanced_rock/axrp-300.pdf`.
6. B. Sharma, W. Brigham, and L. Castanier, "CT imaging techniques for two-phase and three-phase *in situ* saturation measurements," SUPRI TR 107 Report, Contract No. DE-FG22-96BC14994, U.S. Dep. of Energy, June (1997).
7. J. R. Janesick, "Large-area scientific CCDs from memory device to imager," OE Reports No. 110, SPIE–The Int. Soc. for Optical Eng., Bellingham, WA, USA, February (1993).
8. V. N. Vasil'ev, L. A. Levbedev, V. P. Sidorin, and R. V. Stavitskii, *Emission Spectra of X-ray Facilities* [in Russian], Énergoatomizdat, Moscow (1990).
9. A. I. Romanov, "Experimental study of the emission spectra of flash X-ray systems for recording dynamic processes in heterogeneous media," Bachelor's Dissertation, Novosibirsk State University (2003).
10. V. Sundararaman, M. A. Prasad, and R. B. Prasad, "Computed spectra from diagnostic and therapeutic X-ray tubes," *Phys. Med. Biol.*, **18**, No. 2, 208–218 (1973).
11. E. I. Bichenkov, V. L. Ovsiannikov, and E. I. Palchikov, "Dose and duration measurement of X-ray flash dependent on discharge circuit parameters," in: *Proc. of the XI Int. Symp. on Discharge and Electrical Insulation in Vacuum* (Berlin, DDR, 24–28 Sept., 1984), Vol. 2, Berlin, (1984), pp. 451–454; `http://isdeiv.lbl.gov`.
12. "Attenuation and absorption spectra for various media," National Institute of Standards and Technology, Gaithersburg, MD, USA (2005); `http://physics.nist.gov/PhysRefData/XrayMassCoef/`.
13. E. R. Bartuli, A. Yu. Burlev, E. I. Palchikov, and S. V. Sukhinin, " Digital radiographic measurement of the dynamics of spatial fluid distribution in a porous sample," in: *Dynamics of Continuous Media* (collected scientific papers) [in Russian], No. 121, Inst. of Hydrodynamics, Sib, Div., Russian Acad. of Sci., Novosibirsk (2002), pp. 56–69.
14. A. S. Besov, Y. A. Schemelinin, E. I. Palchikov, et al., "Researching the dynamics of movement of gas-fluid mixture in a porous medium by means of low-angle tomography," in: *Proc. of the V Int. Conf. on Multiphase Flow* (Yokohama, Jpn., May 30–June 4, 2004), The University of Tokyo (2004), p. 106; CD-ROM Proc. Paper No. 140.
15. E. I. Palchikov, "Radiographic observation of fluid filtration through an oil-bearing rock," *J. Appl. Mech. Tech. Phys.*, **38**, No. 6, 963–071 (1997).
16. E. I. Palchikov, S. V. Sukhinin, A. Yu. Burlev, et al., "X-ray tomographic flow visualization of multiphase fluid mixture in porous media," in: *Proc. of the VII Triennial Int. Symp. on Fluid Control, Measurement, and Visualization* (Sorrento, Italy, 25–28 Aug., 2003); CD-ROM Proc., ISBN 0-9533991-4-1, Paper No. 101. Publ. Optimage Ltd, Edinburgh; `http://www.vsj.or.jp/jov/Vol7No2/Carlomagno.htm`.